Journal of the Ceramic Society of Japan 121 [10] 907-911 2013 Paper

Facile synthesis of $WO_3 \cdot H_2O$ square nanoplates via a mild aging of ion-exchanged precursor

Mohamed ELNOUBY, Kazuo KURUMA, Eri NAKAMURA, Hiroya ABE,† Yoshikazu SUZUKI* and Makio NAITO

Joining and Welding Research Institute, Osaka University, Ibaraki 567–0047, Japan
***Faculty of Pure and Applied Sciences, University of Tsukuba, Ibaraki 305–8573, Japan**

A facile method to synthesize $WO_3 \cdot H_2O$ square nanoplates via a mild aging (50°C) of ion-exchanged precursor was developed. The ion-exchanged precursor was prepared by passing the sodium tungstate solution (Na_2WO_4) through a protonated cation-exchange resin, and used as impurity-free acidified solution (H_2WO_4) for synthesizing $WO_3 \cdot H_2O$ nanoplates. No shape-directing additive was employed. It was observed that the yellow particles were precipitated under aging at 50°C. After aging for 8 h, the precipitated particles were characterized as the $WO_3 \cdot H_2O$ nanoplates, and their morphological evolution to square platelet proceeded with an increase of aging time. After aging for 24 h, the $WO_3 \cdot H_2O$ square nanoplates were predominantly synthesized. The square nanoplates consisted of a few or several stacked thin layers (thickness, ~10 nm/layer), and provided the well-defined {010} facet for two dominantly exposed surfaces and {101} side facets. Their lateral dimension reached several hundreds of nanometers. It is thus demonstrated that the mild aging (50°C) of the ion-exchanged precursor is a simple and impurity-free synthetic route for $WO_3 \cdot H_2O$ square nanoplates. In addition, the monoclinic WO_3 nanoplates were successfully obtained by dehydration-induced topochemical transformation of the $WO_3 \cdot H_2O$ nanoplates.

Key-words : Tungsten hydrous oxide, Nanostructure, Acid precipitation method, Ion-exchanged precursor

[Received April 30, 2013; Accepted August 7, 2013]

1. Introduction

Tungsten hydrous oxides ($WO_3 \cdot nH_2O$) are the term applied to various solids precipitated by strong acids from a sodium tungstate solution (Na_2WO_4); different crystalline structures as well as morphologies may occur, depending on the processing conditions.[1] Recently, synthetic strategy for nanostructures of $WO_3 \cdot nH_2O$ and their dehydrated WO_3 has been a focused subject due to the interest in both fundamental science and technological applications.[2)–4)] Among various nanostructures, two-dimensional nanoplates have received much attention, because the nanoplates not only can provide active sites for catalysis and sensors[5)–7)] but also can be used as building blocks to construct complex nanostructures.[8)] To date, hydrothermal treatment of the acidified precursor with assistance of shape-directing additives has been widely investigated for synthesizing the nanoplates.[7),9)–12)] However, under the utilization of the acidified precursor, the unavoidably contaminated cations such as Na^+ in the final products may result in negative effects on the performances of materials.[13),14)]

An ion-exchanged precursor is an alternative acidified precursor,[15)] which is prepared by acidification only through a protonated cation-exchange resin. It contains intrinsically negligible amount of by-product ions such as Na^+ and Cl^-, and therefore can be used as impurity-free precursor.[16),17)] It can be also expected that the crystalline $WO_3 \cdot nH_2O$ such as $WO_3 \cdot 2H_2O$ and $WO_3 \cdot H_2O$ would be formed with platelet-morphologies, according to the two-dimensional condensation reaction in the acidified solution (H_2WO_4).[15),18),19)] Nevertheless, there are only a few papers reported on the formation of $WO_3 \cdot nH_2O$ nanoplates in the ion-exchanged precursor. Choi et al.[17)] reported that the ion-exchanged precursor became rapidly turbid, then a gel was formed and transformed into precipitated $WO_3 \cdot 2H_2O$ nanoparticles (about 30 nm in diameter) after three days at room temperature. They found that the precipitates further grew up to be nanoplate morphology by the post-treatments of centrifuging,[20)] ultrasonic agitation[17)] and mixing polyethylene glycol as a shape-director additive.[21)] However, their process needs long route to obtain the nanoplates, and the effect of the process conditions on the morphological evolution has still remained unclear. On the other hand, the hydrothermal treatment (>100°C) promoted rather one-dimensional products like nanorods.[22)] To our knowledge, there have been few efforts to investigate the effect of intermediate or mild aging condition on morphology and structure of $WO_3 \cdot nH_2O$ precipitated in the ion-exchanged precursor.

In this paper, we present a facile and one-pot route to synthesize the square nanoplates of tungsten monohydrous oxide ($WO_3 \cdot H_2O$) via a mild aging of the ion-exchanged precursor at 50°C, without any shape-directing additives. We expect that the synthetic strategy with such a low temperature will receive some benefits as inexpensive and versatile techniques. By using this route, the effect of aging time on the morphological and structural evolution of $WO_3 \cdot H_2O$ nanoplates was investigated. In addition, the WO_3H_2O nanoplates were converted to WO_3 particles by annealing, and their morphology and structure were evaluated.

2. Experimental

2.1 Materials

Sodium tungstate dehydrate ($Na_2WO_4 \cdot 2H_2O$, >99%) was purchased from Kanto Chemicals Co. (Japan) and were used without further purification. Strong acid type of Diaion PK228LH cation exchange resin (ion-exchange capacity >2.05 meq/ml) was supplied from Mitsubishi Chemical Co. (Japan). Deionized water (18.2 MΩcm) from Sartorius-arium® 61316 system (Germany) was used throughout the experiments.

† Corresponding author: H. Abe; E-mail: h-abe@jwri.osaka-u.ac.jp

DOI http://dx.doi.org/10.2109/jcersj2.121.907

A glass column with height of 150 mm and 24.6 mm in diameter was used for the ion-exchange process. The glass column was packed with 30 mL of the ion-exchange resin, and then 10 mL of water was passed through the column to wash the resin. This washing step was repeated five times before the experiment.

2.2 Sample preparations

0.5 M Na_2WO_4 solution was prepared by dissolving $Na_2WO_4 \cdot 2H_2O$ powder into deionized water. Then, a 10 mL of the solution was loaded on the glass column, and the acidified tungstic acid (H_2WO_4) solution was recovered from the column by elution with deionized water. The resulting H_2WO_4 solution was yellowish and transparent. The concentration of H_2WO_4 was determined to be 0.23 M by X-ray fluorescence spectroscopy (EDX-800, Shimazu, Japan).

The solution was aged at 50°C by employing four different aging times of 8, 16, 24 and 168 h. No additive was used in this experiment. After aging, the precipitated powder was collected for morphological and structural examinations. Furthermore, WO_3 nanoparticles were synthesized by annealing the $WO_3 \cdot H_2O$ samples at 350°C in air for 1 h.

2.3 Characterizations

The crystallographic phase of the samples was determined by powder X-ray diffraction (XRD; Ultima IV, Rigaku, Japan, Cu-Kα radiation). Their morphology were examined by scanning electron microscopy (SEM; JSM 6010LA, JEOL, Japan) and atomic force microscopy (AFM; NanoNavi Station, SII, Japan). Their microstructures were also observed by transmission electron microscopy (TEM; JEM-2100F, JEOL, Japan). The weight loss of the precipitate was measured by a thermogravimetric analysis (TG; TG/DTA 6200, SII, Japan). The structural property of WO_3 obtained by annealing the $WO_3 \cdot H_2O$ sample was evaluated by XRD and TEM analyses.

3. Results and discussion

3.1 Synthesis of $WO_3 \cdot H_2O$ square nanoplates

Under aging the ion-exchanged precursor at 50°C, the yellow precipitate was observed at the bottom of solution. **Figure 1** shows the XRD patterns of the precipitates obtained after aging times of 8, 16, 24, and 168 h. All peaks in the four XRD patterns were indexed to the orthorhombic $WO_3 \cdot H_2O$ phase with space group of *Pmnb* (62) and lattice parameters $a = 5.2380$ Å, $b = 10.7040$ Å, $c = 5.1200$ Å (ICDD Card No. 00-043-0679). No secondary phase was detected for all samples. It should be noted that the intensity ratio of (020) to (111) reflection peaks increased with an increase of the aging time, suggesting that the products show a preferential orientation of the (020) crystal plane.

Figure 2 shows the SEM images of the $WO_3 \cdot H_2O$ samples obtained after aging time of 8, 16, 24 and 168 h. It is revealed that all samples are composed of a large quantity of nanoplates. The size of the nanoplates did not significantly increase with an increase of aging time, even after prolonging aging time to 168 h and it was of several hundreds of nanometers. On the other hand, the morphology of the particles changes from relatively round shape (8 h) to square shape with increase of aging time. The present observation indicates that the aging time plays an

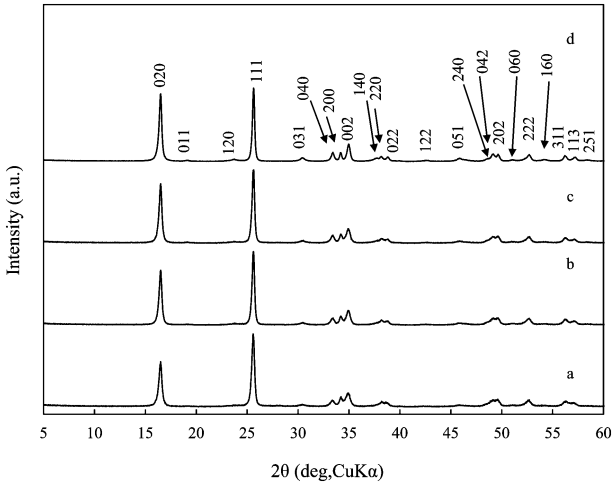

Fig. 1. XRD patterns of as-prepared tungsten oxide aged at 50°C for (a) 8 h (b) 16 h (c) 24 h (d) 168 h [all peaks can be indexed to $WO_3 \cdot H_2O$ (ICDD No. 00-043-0679)].

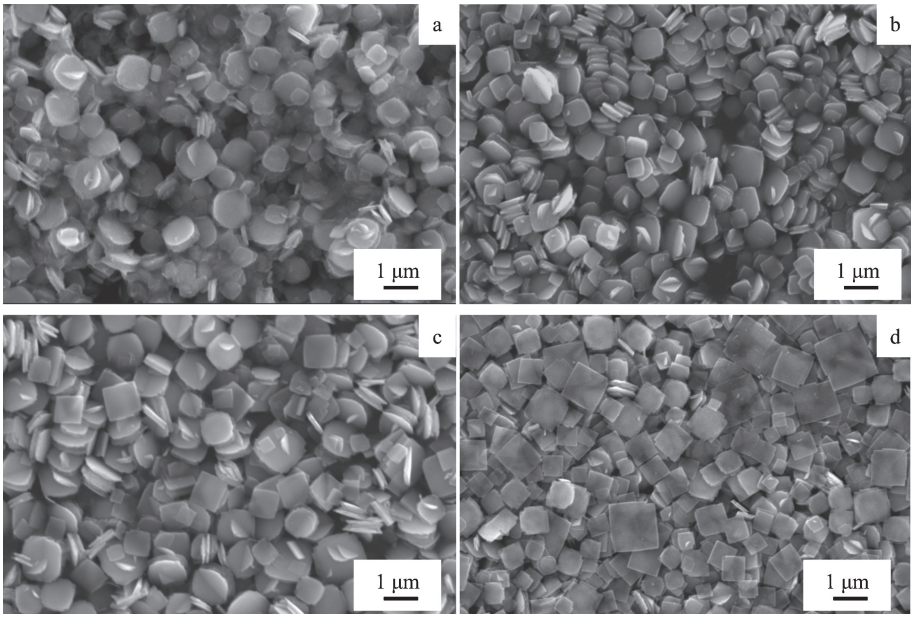

Fig. 2. SEM images of $WO_3 \cdot H_2O$ nanoplates aged at 50°C for (a) 8 h (b) 16 h (c) 24 h (d) 168 h.

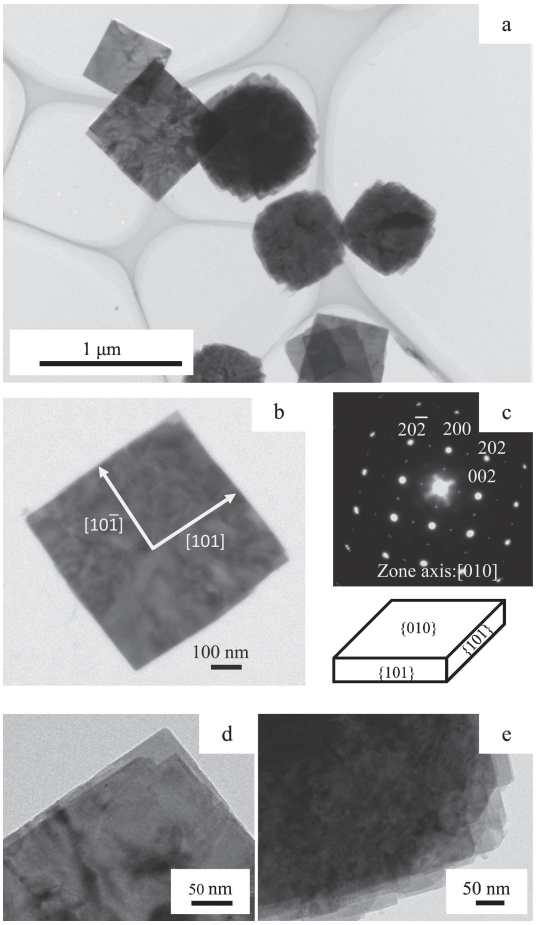

Fig. 3. (a) TEM images of $WO_3 \cdot H_2O$ nanoplates (b, c) TEM image of $WO_3 \cdot H_2O$ nanoplate and its corresponding SAED pattern, with crystalline model of the nanoplate (d, e) magnified TEM images of the edge of $WO_3 \cdot H_2O$ nanoplates.

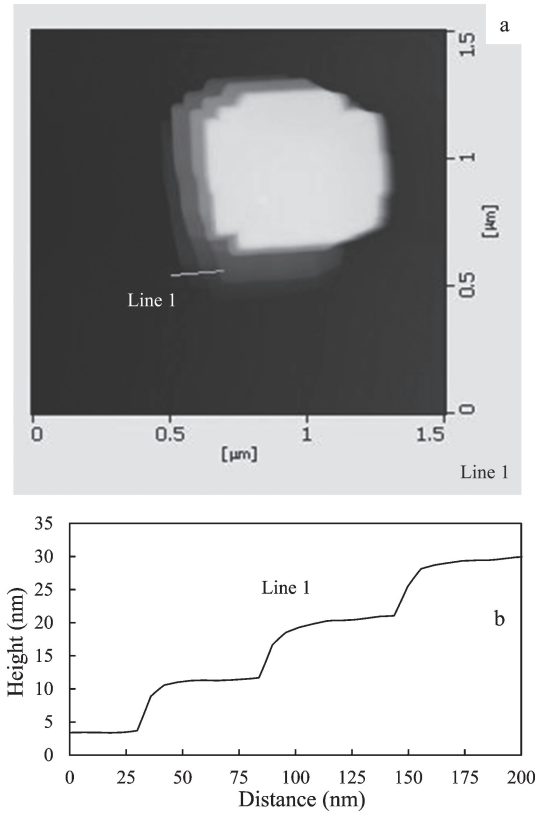

Fig. 4. (a) AFM image of a $WO_3 \cdot H_2O$ nanoplate (b) Height profile along "line 1" in (a).

important role on the formation of $WO_3 \cdot H_2O$ square nanoplates, and a suitable reaction time was 24 h and more.

Figure 3(a) show a typical TEM image of the square nanoplates obtained after ageing time of 24 h. The square nanoplates were clearly observed from the TEM image. The lateral dimension of the nanoplates reached several hundreds of nanometers. Figure 3(b) is a typical set of TEM image and the corresponding SAED pattern. All other nanoplates also showed the identical SAED pattern which can be assigned to a phase of single crystalline of the orthorhombic $WO_3 \cdot H_2O$ located along the [010] zone axis, revealing that it provides the well-defined {010} facet for two dominantly exposed surfaces. In addition, the [101] and [10$\bar{1}$] directions are almost perpendicular to adjacent sides of the square nanoplates, indicating the nanoplates are enclosed by {101} facets on four sides. From these observations, it can be concluded that the $WO_3 \cdot H_2O$ precipitated grows preferentially along to {010} plane and eventually is enclosed by {101} side facets to form square platelets under aging at 50°C. Figures 3(b) and 3(c) shows higher magnified images of the $WO_3 \cdot H_2O$ nanoplates. It can be seen that these nanoplates are not monolayer, but consisted of a few or several stacked nanosheets.

Figures 4(a) and 4(b) show an AFM image of a $WO_3 \cdot H_2O$ nanoplate and the cross-sectional profile corresponds to the line drawn in (a), respectively. The observed topographical feature along the line suggests that the at least three thin layers stacked and each layer is of around 10 nm in thickness.

In this study, we focused on the mild aging for controlling morphology and structure of the precipitates in the ion-exchanged precursor, and demonstrated that the $WO_3 \cdot H_2O$ square nanoplates were successfully synthesized. In the previous studies, the precipitates were often obtained under aging at room temperature[15),17)] and they were identified as $WO_3 \cdot 2H_2O$. Their morphology was not well-developed nanoplates (nanoparticles) even after aging for three days,[17)] indicating that the crystal growth did not efficiently proceeded under room temperature. On the other hand, hydrothermal treatment (180°C for 24 h) promoted rather one-dimensional crystal growth, resulting in the hexagonal WO_3 and $WO_3 \cdot 1/3H_2O$ with nanorod morphology.[22)] It is thus proven that the present aging temperature is adequate to synthesize the $WO_3 \cdot H_2O$ square nanoplate in the impurity-free acidified precursor.

Since the present ion-exchanged precursor contained negligible amount of impurity-ions and no shape-directing additives, i.e., contained no extra species which may influence crystal growth, the observed preferential growth of $WO_3 \cdot H_2O$ along to {010} plane can be explained from the intrinsic growth habit of $WO_3 \cdot H_2O$ as follows: at the initial period of aging, the intermediate $[WO(OH)_4(OH)_2]$ are formed in acidified solution (H_2WO_4),[9),15)] where one water molecule is bonded along to the *b*-axis opposite to the W=O bond while the four OH groups are in the equatorial *a*-*c* plane. Then, the intermediates condense to form a $[WO_5(OH_2)]$ octahedral layer through oxolation reaction along to the equivalent *a*- and *c*- directions, i.e., along to {010} plane.[15),19)] The $[WO_5(OH_2)]$ octahedral layers are bonded to each other by hydrogen bonds between the terminal oxygen and coordinated water molecules in neighboring layers, leading to the formation of a layered and platelet $WO_3 \cdot H_2O$ structure. From the

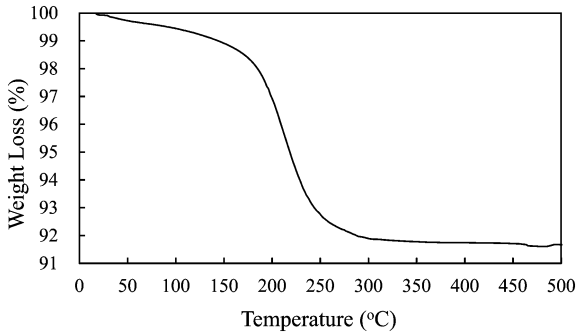

Fig. 5. TGA curve of $WO_3 \cdot H_2O$ nanoplates.

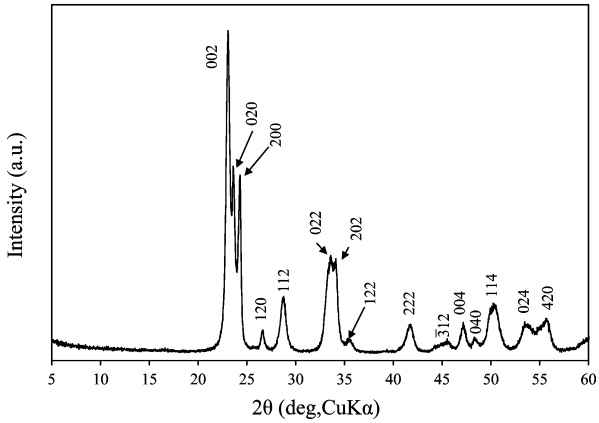

Fig. 6. XRD pattern of WO_3 nanoplates after annealing at 350°C for 1 h [all peaks can be indexed to monoclinic WO_3 (ICDD No. 01-072-0677)].

above consideration, the present aging temperature definitely promotes the two-dimensional oxolation reaction, i.e., extending $[WO_5(OH_2)]$ octahedral layer which cause the formation nanoplatelets. However, the detailed mechanism of formation of the $WO_3 \cdot H_2O$ square nanoplates needs to be further explored.

3.2 Dehydration behavior of $WO_3 \cdot H_2O$ square nanoplates

Figure 5 shows the weight loss behavior of the $WO_3 \cdot H_2O$ nanoplates for temperatures from 25 and 500°C measured by TGA. From the figure, it is clear that the $WO_3 \cdot H_2O$ nanoplates had an obvious weight loss around 200°C. The amount of the structural water of the precipitate can be calculated from the weight loss difference between 150 and 500°C, with taking account of physically adsorbed water. As a result, it corresponded to about $1H_2O$ per mole of WO_3.

Figure 6 shows the XRD pattern of the annealed sample. All XRD peaks were indexed to monoclinic WO_3 phase (ICDD Card No. 01-072-0677). **Figures 7**(a) and 7(b) show a typical TEM image and its corresponding SAED pattern of one of the annealed WO_3. As shown in the figure, the WO_3 square nanoplate was formed from the $WO_3 \cdot H_2O$ nanoplate without obvious morphological change. In the corresponding SAED pattern, the uniform, wide and ordered diffraction spots can be assigned to a phase of single-crystal monoclinic WO_3 located along the [001] zone axis. Since the WO_3 nanoplate is lying flat on the TEM grid, the thickness of the WO_3 nanoplate is definitely the [001] direction. [100] and [010] directions are almost perpendicular to adjacent sides of the square. These observations reveal that the dehydrated WO_3 square nanoplate provides the well-defined {001} facet

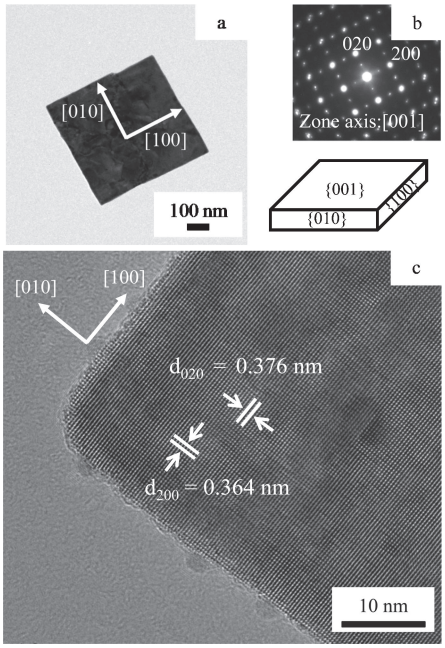

Fig. 7. (a, b) TEM image of WO_3 nanoplate and its corresponding SAED pattern, with crystalline model of the nanoplate (c) HRTEM image of WO_3 nanoplate.

for two dominantly exposed surfaces with {100} and {010} side facets.

Figure 7(c) shows HRTEM image of the edge of the WO_3 nanoplate. The clear two dimensional ordered lattice fringe means that the obtained WO_3 nanoplate is a single crystal. The interplanar distance values of 0.364 and 0.376 nm can be assigned to the (200) and (020) crystal planes of monoclinic WO_3, respectively.

During the annealing, the coordinated water molecules between the $[WO_5(OH_2)]$ octahedral layers in $WO_3 \cdot H_2O$ nanoplates were driven out to stabilize the system three-dimensionally and monoclinic WO_3 began to form. The morphology of square nanoplate could be maintained during the dehydration process, which is considered to be a topotactic process. The structural evolution of [010] oriented $WO_3 \cdot H_2O$ nanoplates to [001] oriented WO_3 nanoplates can be simply explained by the crystallographic topotaxy, based on their similarity of the W–O octahedral layers in both $WO_3 \cdot H_2O$ and WO_3.[11)]

4. Conclusions

We have investigated the effect of mild aging (50°C) on the morphology and structure of $WO_3 \cdot nH_2O$ precipitated in the ion-exchanged precursor without any shape-directing additives, and found that the $WO_3 \cdot H_2O$ square nanoplates can be synthesized for 24 h. The nanoplates consisted of stacked thin nanosheet (~10 nm) which provided the well-defined {010} facet for two dominantly exposed surfaces. The lateral dimension of the nanoplates reached several hundreds of nanometers. In addition, WO_3 nanoplates were successfully obtained by dehydration-induced topochemical transformation of $WO_3 \cdot H_2O$ nanoplates at 350°C in air. The obtained $WO_3 \cdot H_2O$ square nanoplates and WO_3 ones are expected for their wide applications such as sensors and building blocks for constructing functional nanostructures.

Acknowledgments This work was supported by Grand-in-Aid for Scientific Research (B) (KAKENHI No. 23360323) from the

Ministry of Education, Culture, Sports, Science and Technology of Japan and by the Cooperative Research Program of Institute for Joining and Welding Research Institute, Osaka University.

References

1) B. Gerand, G. Nowogrocki and M. Figlarz, *J. Solid State Chem.*, **38**, 312–320 (1981).
2) J. Shi, G. Hu, R. Cong, H. Bu and N. Dai, *New J. Chem.*, **37**, 1538–1544 (2013).
3) Y. P. Xie, G. Liu, L. Yin and H.-M. Cheng, *J. Mater. Chem.*, **22**, 6746–6751 (2012).
4) X. Liu, F. Wang and Q. Wang, *Phys. Chem. Chem. Phys.*, **14**, 7894–7911 (2012).
5) X. Chen, Y. Zhou, Q. Liu, Z. Li, J. Liu and Z. Zou, *Appl. Mater. & Inter.*, **4**, 3372–3377 (2012).
6) O.-u. Nimittrakoolchai and S. Supothina, *Mater. Chem. Phys.*, **112**, 270–274 (2008).
7) S.-J. Kim, I.-S. Hwang, J.-K. Choi and J.-H. Lee, *Thin Solid Films*, **519**, 2020–2024 (2011).
8) K. K-zadeh, A. Vijayaraghavan, M.-H. Ham, H. Zheng, M. Breedon and M. S. Strano, *Chem. Mater.*, **22**, 5660–5666 (2010).
9) J. Yang, W. Li, D. Sun and Q. Chen, *J. Mater. Chem.*, **22**, 17747–17752 (2012).
10) X. Su, F. Xiao, Y. Li, J. Jian, Q. Sun and J. Wang, *Mater. Lett.*, **64**, 1232–1234 (2010).
11) J. Ma, J. Zhang, S. Wang, T. Wang, J. Lian, X. Duan and W. Zheng, *J. Phys. Chem. C*, **115**, 18157–18163 (2011).
12) H.-F. Pang, X. Xiang, Z.-J. Li, Y.-Q. Fu and X.-T. Zu, *Phys. Status Solidi A*, **209**, 537–544 (2012).
13) H. Zhang, G. Duan, Y. Li, X. Xu, Z. Dai and W. Cai, *Cryst. Growth Des.*, **12**, 2646–2652 (2012).
14) K. O. Iwu, A. Galeckas, P. Rauwel, A. Y. Kuznetsov and T. Norby, *J. Solid State Chem.*, **185**, 245–252 (2012).
15) J. Livage and G. Guzman, *Solid State Ionics*, **84**, 205–211 (1996).
16) M. Gotic, M. Ivanda, S. Popovic and S. Music, *Mater. Sci. Eng., B*, **B77**, 193–201 (2000).
17) Y.-G. Choi, G. Sakai, K. Shimanoe, N. Miura and N. Yamazoe, *Sens. Actuators, B*, **87**, 63–72 (2002).
18) J. Livage and D. Ganguli, *Sol. Energy Mater. Sol. Cells*, **68**, 365–381 (2001).
19) M. Breedon, P. Spizzirri, M. Taylor, J. Plessis, D. MacCulloch, J. Zhu, L. Yu, Z. Hu, C. Ric, W. Wlodarski and L. Kalantar-zadeh, *Cryst. Growth Des.*, **10**, 430–439 (2010).
20) Y.-G. Choi, G. Sakai, K. Shimanoe, Y. Teraoka, N. Miura and N. Yamazoe, *Sens. Actuators, B*, **93**, 486–494 (2003).
21) Y.-G. Choi, G. Sakai, K. Shimanoe, Y. Teraoka and N. Yamazoe, *Sens. Actuators, B*, **101**, 107–111 (2003).
22) R.-F. Mo, G.-Q. Jin and X.-T. Guo, *Mater. Lett.*, **61**, 3787–3790 (2007).